Fig. 4. Radiation patterns of the double-layered CPAs at 10 GHz (a) AUT A. (b) AUT B. (c) AUT C. (d) AUT D. ——— H-plane co-polarization, × × × × × H-plane cross-polarization, — — — — E-plane co-polarization, ● ● ● ● ● E-plane cross-polarization.

was 9.4 dBi within the pass band. The radiation patterns were stable and the maximum cross-polarization level of the antenna was about − 18 dB.

REFERENCES

[1] P. Otero, G. V. Eleftheriades, and J. R. Mosig, "Integrated modified rectangular loop slot antenna on substrate lenses for millimeter- and sub-millimeter-wave frequencies mixer applications," *IEEE Trans. Antennas Propagat.*, vol. 46, pp. 1489–1497, Oct. 1998.

[2] S. Sierra-Garcia and J.-J. Laurin, "Study of a CPW inductively coupled slot antenna," *IEEE Trans. Antennas Propagat.*, vol. 47, pp. 58–64, Jan. 1999.

[3] W. Menzel and W. Grabherr, "A microstrip patch antenna with coplanar feed line," *Microwave Guided Wave Letters*, vol. 1, no. 11, pp. 340–342, Nov. 1991.

[4] B. K. Kormanyos, W. Harokopus Jr., L. P. B. Katehi, and G. M. Rebeiz, "CPW-fed active slot antennas," *IEEE Trans. Microwave Theory Techniques*, vol. 42, pp. 541–545, Apr. 1994.

[5] H.-C. Liu, T.-S. Horng, and N. G. Alexopoulos, "Radiation of printed antennas with a coplanar waveguide feed," *IEEE Trans. Antennas Propagat.*, vol. 43, pp. 1143–1148, Oct. 1995.

[6] L. Giauffret, J.-M. Laheurte, and A. Papiernik, "Study of various shapes of the coupling slot in CPW-fed microstrip antennas," *IEEE Trans. Antennas Propagat.*, vol. 45, pp. 642–647, Apr. 1997.

[7] K. Li, C. H. Cheng, T. Matsui, and M. Izutsu, "Coplanar patch antennas: Principle, simulation and experiment," in *Proc. IEEE AP-S Symp.*, vol. 3, Boston, MA, July 2001, pp. 406–409.

[8] K. F. Tong, K. Li, T. Matsui, and M. Izutsu, "Wideband coplanar waveguide fed coplanar patch antenna," in *Proc. IEEE Antennas and Propagation Society Int. Symp.*, vol. 3, Boston, MA, July 2001, pp. 406–410.

[9] R. N. Simons, *Coplanar Waveguide Circuits, Components, and Systems*, ser. Wiley Series in Microwave & Optical Engineering. Los Alamitos, CA: IEEE Comput. Soc. Press, 2001, vol. 1304, ch. 3, pp. 88–89.

Analysis of an Arbitrary Conic Section Profile Cylindrical Reflector Antenna, H-Polarization Case

Taner Oğuzer, Alexander I. Nosich, and Ayhan Altintas

Abstract—Two-dimensional scattering of waves by a perfectly electric conducting reflector having arbitrary smooth profile is studied in the H-polarization case. This is done by reducing the mixed-potential integral equation to the dual-series equations and carrying out analytical regularization. To simulate a realistic primary feed, directive incident field is taken as a complex source point beam. The proposed algorithm shows convergence and efficiency. The far field characteristics are presented for the reflectors shaped as quite large-size curved strips of elliptic, parabolic, and hyperbolic profiles.

Index Terms—Analytical regularization, complex source, reflector antenna.

I. INTRODUCTION

One of the most important segments of rapidly developing wireless communication systems is open-space propagation. In this research area the reflector antenna simulation, design and sophistication plays an important role because reflectors (Fig. 1) are one the best choices among the antennas with high directivity [1]. Besides, shaped radiation patterns are frequently needed or the beam can be focused on a near-zone target. In these configurations the reflectors may have elliptic, hyperbolic, parabolic or other specialized surfaces. Therefore it
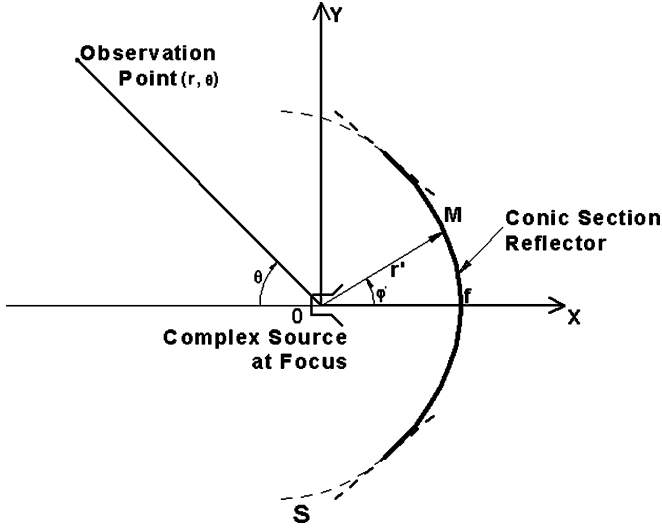
Fig. 1.   Geometry of the 2-D reflector antenna system with the complex source at the focus of the arbitrary conic section reflector.

is highly desired to have a quick and accurate simulation tool, which can be further implemented in a numerical-optimization code, to find the reflector and feed parameters providing a desired radiation performance.

Even though the real-life antennas have three-dimensional (3-D) reflector surfaces, sometimes almost 2-D ones are used in the communication and airborne earth scanning systems. As the whole idea of reflector had been borrowed from optics, quasioptical (QO) methods combining ray tracing with approximate account of the edge diffraction are widely used in simulations. These methods mainly depend on the asymptotic solution of canonical structures, e.g., a half plane. Then the reflection and diffraction coefficients appear in the ray format and further can be used in solving more complicated geometries. E.g., a 2-D reflector illuminated with a directive feed was modeled in [2] with QO techniques in the form of the uniform theory of diffraction and aperture integration, combined with the complex source point (CSP) method [3]. In [4], the scattering from a 2-D circular strip was treated analytically with the Wiener–Hopf method assuming the size of the strip to be asymptotically large. However, these analyses failed to take into account all scattering mechanisms and their possible higher-order interactions together. Another way of the solution is to use numerical techniques like the method of moments (MoM) with simple locally defined basis functions. MoM can be applied to the small and medium-size problems and provides the accuracy within a few digits [5]. However, larger geometries or better accuracy values quickly hit nonrealistic computer time requirements that has led to the invention of the fast multipole method. Nevertheless, the fundamental problem is that here the convergence of solving singular IEs with MoM is not guaranteed mathematically [6].

Therefore, development of an accurate and economic method for the simulation of arbitrary 2-D reflector antennas is still of great interest. This can be done by using the method of analytical regularization (MAR) [7]—for solving IE, and the CSP method—for simulating the feed field. Here, MAR is based on the explicit inversion of the most singular part of electric field integral equation (EFIE). This can be done either in the space domain, with the weighted Chebyshev polynomials as expansion functions [8], or in the discrete-Fourier-transform domain, with full-period exponents (also known as trigonometric polynomials) as a basis. In the latter case, a specialized function-theoretic technique called the Riemann–Hilbert problem (RHP) method is known to be useful [9]–[12]. In [13], we studied a perfectly electric

conducting (PEC) 2-D circular reflector antenna in free space by combining CSP with MAR-RHP in one accurate technique. Later the same approach was extended to study imperfect edge-loaded reflector [14], reflector in a circular dielectric radome [15], [16], and reflector above impedance flat earth [17]. Further, more realistic reflector surfaces can be also considered, with a general profile given by a twice-differentiable open curve. In [18], such a reflector was solved in the E-polarization case by following the ideas of [19] and using the MAR-RHP technique. One of the basic steps here was to introduce an auxiliary circle that was smoothly joined with the reflector contour, and to exploit the semi-inversion of equations for a circularly curved strip. Relevant papers [20]–[22] worked with similar ideas and used the theory of the Abel IE and the dual-series equations (DSE) in terms of the Jacobi polynomials, although no numerical data were given.

Below we shall formulate the IE for a 2-D reflector with arbitrary profile by using the auxiliary vector and scalar potentials. Such a mixed-potential integral equation (MPIE) is attractive as being less singular than EFIE—in our case it has at most Cauchy-type singularity. Then MPIE is cast into a DSE format and regularized by using RHP technique, which leads to a matrix equation of the Fredholm second kind.

II. FORMULATION

The geometries that we shall study are PEC cylindrical reflectors having arbitrary conical section profiles, i.e., elliptic, parabolic, or hyperbolic ones. A directive incident beam field located at one of the focuses illuminates such a zero-thickness reflector in symmetric manner (see Fig. 1). The origin of the used coordinate system $(x, y) = (r, \varphi)$ is taken just in this focus, and the point O_e or O_h represents the symmetry center of the ellipse or hyperbola, respectively, while the focal distance is taken as $f = |a_{e,h} - c|$ (see Figs. 2 and 3). The parabola can be considered as the limit case of the ellipse, i.e., $e \to 1$. In this case one focus of the ellipse goes to infinity and the other one remains fixed as the focus of parabola. All these curves can be represented by the same equation, namely

$$y^2 + (1 - e^2)x^2 + 2fe(1 + e)x = f^2(1 + e)^2 \qquad (1)$$

where $e = c/a_{e,h}$ is the eccentricity factor of the curve and defines a circle ($e = 0$), ellipse ($0 < e < \infty$), parabola ($e = 1$) or hyperbola ($1 < e < \infty$). When building the solution, an open arc M of this generalized curve (representing reflector's cross section) is completed to a closed contour C by adding a circular arc S of the radius a_s having its center shifted at a distance L from the origin on the negative x-axis. The radius a_s and the distance L are chosen in such a way that at the connection points $(r_e, \pm\theta_e)$ the curvatures of the arcs M and S are matched. As a result, the closed contour first derivatives are continuous, and discontinuities in the second derivatives are finite. We will see that this is essential to reduce our problem to a regularized matrix equation.

The requirements for the unique solution of the presented boundary value problem are stated as follows: the field function has to satisfy the Helmholtz equation off M, Sommerfeld's radiation condition, PEC boundary condition on M, and the edge condition. In the considered case of H-polarization, the tangential scattered electric field can be written by using the auxiliary potentials depending on the tangential surface current J_t, and by imposing the PEC boundary condition on M, i.e., $E_t^{sc} = -E_t^{in}$, one obtains the following MPIE [25]

$$-E_t^{in}(\vec{r}) = \frac{iZ_0}{k} \frac{\partial}{\partial l} \int_M \left(\frac{\partial}{\partial l'} J_{t'}(\vec{r}') \right) G_O(\vec{r}, \vec{r}') dl'$$

$$+ ikZ_0 \int_M J_{t'}(\vec{r}') \cos\left(\xi(\vec{r}) - \xi(\vec{r}')\right) G_O(\vec{r}, \vec{r}') dl' \quad (2)$$
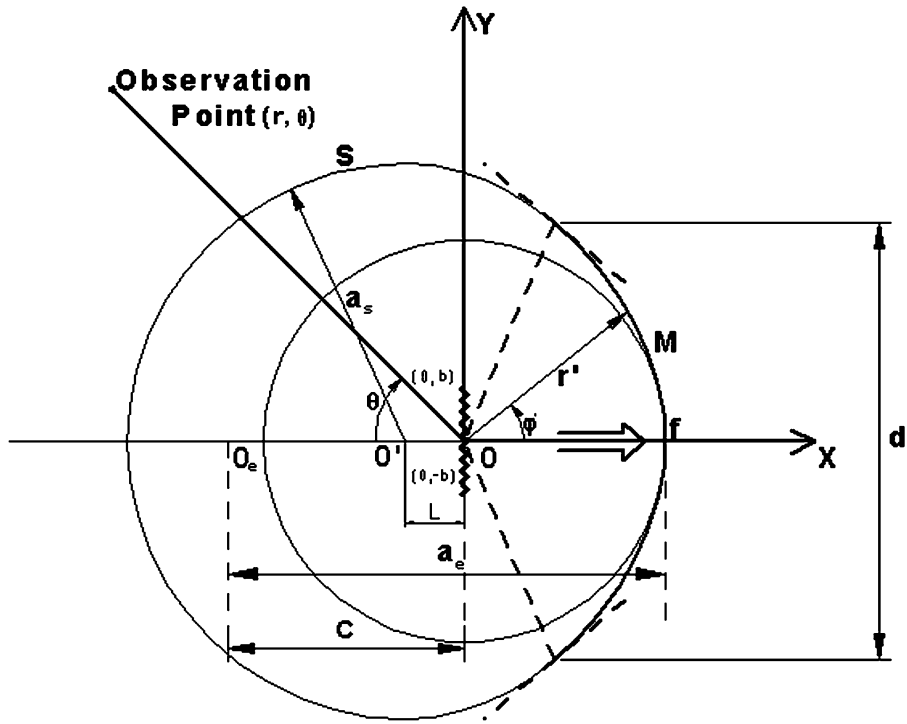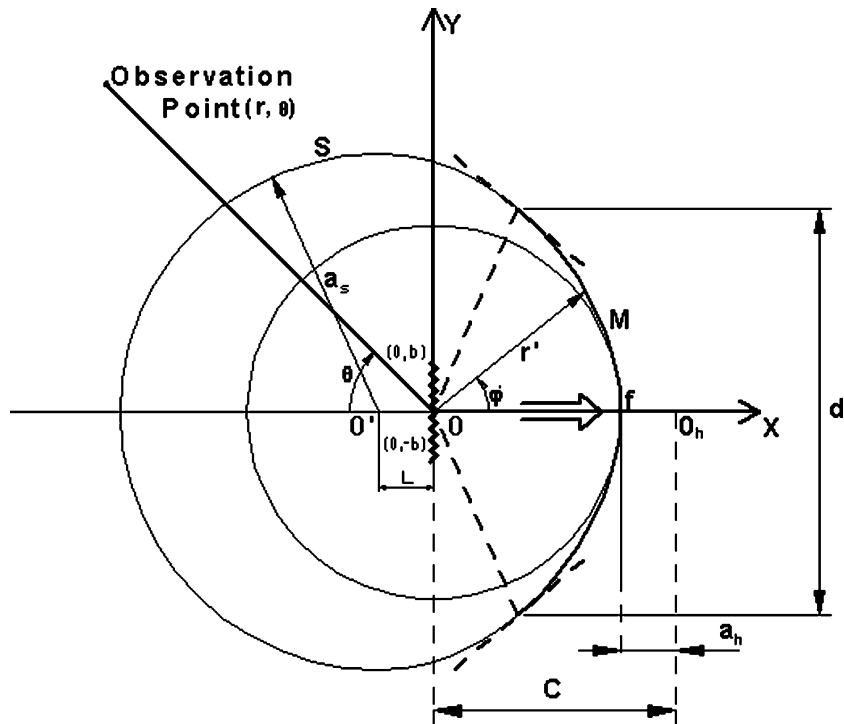
Fig. 2. Geometry of the antenna with elliptic reflector.

Fig. 3. Geometry of the antenna with hyperbolic reflector.

where $k = \omega\sqrt{\mu_0\varepsilon_0}$ is the free space wave number, $E_t^{\text{in}}(\vec{r}) = -(iZ_0/k)(\partial H_z^{\text{in}}/\partial n)$, $G_0 = (i/4)H_o^{(1)}(k|\vec{r} - \vec{r}\,'|)$, and $\vec{n}$ is the outer unit normal vector. Suppose now that the arc M can be characterized by parametric equations in terms of the polar angle, $x = x(\varphi)$, $y = y(\varphi)$, where $-\theta_e \leq \varphi \leq \theta_e$. Besides, define the differential lengths in the tangential direction at any point on M as $\partial l = a\beta(\varphi)\partial\varphi$, $\partial l' = a\beta(\varphi')\partial\varphi'$, respectively. Here, $\beta(\varphi) = r(\varphi)/(a\cos\gamma(\varphi))$, $\xi(\varphi)$ is the angle between the normal on M and the x-direction, $\gamma(\varphi)$ is the angle between the normal and the radial direction, and a is the radius of the auxiliary circle taken here equal to the focal distance f.

After the multiplication of the both sides of (2) with $a\beta(\varphi)$, the MPIE is cast to the following form:

$$
\frac{\partial}{\partial \varphi} \int_{-\theta_e}^{\theta_e} \frac{\partial J_{t'}(\varphi')}{\partial \varphi'} G_0(\varphi, \varphi') d\varphi'
$$
$$
+ (ka)^2 \int_{-\theta_e}^{\theta_e} J_{t'}(\varphi') \cos\left(\xi(\varphi) - \xi(\varphi')\right)
$$
$$
\times \beta(\varphi)\beta(\varphi') G_0(\varphi, \varphi') d\varphi' = a\beta(\varphi) \frac{\partial H_z^{\text{in}}}{\partial n}, \quad \varphi \in M \qquad (3)
$$

where $r(\varphi) = f(1+e)/(1+e\cos(\varphi))$ describes the position vector for all conic section profiles depending on the eccentricity factor e. Note that MPIE (3) suggests that the current $J_t(\varphi)$ is a continuously differentiable function on M.

To follow the common procedure of RHP technique [9]–[12], we have to convert (3) to the discrete-Fourier-transform domain. First of all, we extend the current density function by zero value on S and change integration domain in (3) from M to C (i.e., from 0 to 2π in φ'). Then, the unknown function J_t is discretized with the mentioned exponents as

$$
J_{t'}(\varphi') = \sum_{n=-\infty}^{\infty} x_n e^{in\varphi'}, \quad \varphi' \in C \qquad (4)
$$

and further it will be assumed that this series converges uniformly and hence can be differentiated in term-by-term manner.

Further the following auxiliary regular functions are introduced:

$$
H(\varphi, \varphi') = H_0^{(1)}\left(k\left|\vec{r}(\varphi) - \vec{r}(\varphi')\right|\right) - H_0^{(1)}\left(2ka\left|\frac{\sin(\varphi - \varphi')}{2}\right|\right)
$$
$$
G(\varphi, \varphi') = \cos\left(\xi(\varphi) - \xi(\varphi')\right)\beta(\varphi)\beta(\varphi')H_0^{(1)}
$$
$$
\times \left(k\left|\vec{r}(\varphi) - \vec{r}(\varphi')\right|\right) - \beta^2(\varphi)H_0^{(1)}
$$
$$
\times \left(2ka\left|\frac{\sin(\varphi - \varphi')}{2}\right|\right). \qquad (5)
$$

Now we can modify (3) as follows:

$$
\frac{\partial}{\partial \varphi} \int_{-\theta_e}^{\theta_e} \frac{\partial J_{t'}(\varphi')}{\partial \varphi'} H(\varphi, \varphi') d\varphi'
$$
$$
+ \frac{\partial}{\partial \varphi} \int_{-\theta_e}^{\theta_e} \frac{\partial J_{t'}(\varphi')}{\partial \varphi'} H_0^{(1)}\left(2ka\sin\left(\frac{|\varphi - \varphi'|}{2}\right)\right) d\varphi'
$$
$$
+ (ka)^2 \int_{-\theta_e}^{\theta_e} J_{t'}(\varphi') G(\varphi, \varphi') d\varphi'
$$
$$
+ (ka)^2 \beta^2(\varphi) \int_{-\theta_e}^{\theta_e} J_{t'}(\varphi') H_0^{(1)}
$$
$$
\times \left(2ka\sin\left(\frac{|\varphi - \varphi'|}{2}\right)\right) d\varphi' = \frac{4}{i} a\beta(\varphi) \frac{\partial H_z^{\text{in}}}{\partial n}; \quad \varphi \in M. \quad (6)
$$

The above IE is built by adding and subtracting the explicitly given terms from the actual kernels of the original MPIE. These terms appear in the left side of the (6) inside the second and fourth integrals and include the free space Green's function defined on the auxiliary circle of radius a, therefore $H(\varphi, \varphi')$ and $G(\varphi, \varphi')$ are regular if $\varphi, \varphi' \in S \times S$.

The most singular part of the IE is inside the second integral. Here, a Cauchy-type singularity appears from the derivative of the logarithm, however, it is invertible by the RHP technique when IE is moved to the discrete-Fourier-transform domain. If φ approaches φ', the $H(\varphi, \varphi')$ and $G(\varphi, \varphi')$ functions have also continuous first derivatives, and their second derivatives with respect to s and s' have only logarithmic singularities and hence belong to L_2. The mentioned functions are expanded into the double Fourier series with respect to two arguments producing coefficients h_{nm} and g_{nm}, respectively. The above mentioned conditions imposed on curve C entail that these coefficients asymptotically decay as $O(|n|^{-1.5-\varepsilon}|m|^{-1.5-\varepsilon})$—see [24]. Their efficient computation needs double integration of rapidly oscillating functions that is done with the double fast-Fourier transform (FFT). In this way one can solve electrically large geometries in accurate manner within a reasonable time [24].

The incident field produced by the CSP feed is given by the complex-argument Hankel function

$$
H_z^{\text{in}} = H_0^{(1)}\left(k|\vec{r} - \vec{r}_{cs}|\right) \qquad (7)
$$

where $\vec{r}_{cs} = \vec{r}_0 + i\vec{b}$, $\vec{r}_0$ is the real position vector and $i\vec{b}$ is the complex vector, which characterizes the beam direction and its width—see [2], [3], [13]–[18]. The right-hand part of (3) is expanded into the Fourier series as follows:

$$
\left(\frac{\partial H_z^{\text{in}}}{\partial n}\right) a\beta(\varphi) = -ka\beta(\varphi)\left(\frac{\partial R_{cs}}{\partial n}\right) H_1^{(1)}(kR_{cs})
$$
$$
= \sum_{n=-\infty}^{\infty} z_n e^{in\varphi} \qquad (8)
$$

where $R_{cs} = |\vec{r} - \vec{r}_{cs}|$, $\vec{r}_{cs} = \hat{a}_x (r_0 + ib)$. In the computations we shall assume that $r_0 = 0$, and the vector $\vec{b}$ is orientated in the x-direction.

Discretization of (6), together with equation $J_t(\varphi) = 0$, $\varphi \in S$ leads to the following DSE for the unknown coefficients:

$$
\sum_{n=-\infty}^{\infty} x_n |n|^2 J_n(ka) H_n^{(1)}(ka) e^{in\varphi}
$$
$$
+ \sum_{n=-\infty}^{\infty} e^{in\varphi} \sum_{p=-\infty}^{\infty} x_p p n h_{n(-p)} - (ka)^2 \sum_{n=-\infty}^{\infty} e^{in\varphi}
$$
$$
\times \sum_{p=-\infty}^{\infty} x_p \left[J_p(ka) H_p^{(1)}(ka)\beta_{n-p} + g_{n(-p)}\right]
$$
$$
= \frac{2i}{\pi} \sum_{n=-\infty}^{\infty} z_n e^{in\varphi}, \quad \varphi \in M
$$
$$
\sum_{n=-\infty}^{\infty} x_n e^{in\varphi} = 0, \quad \varphi \in S \qquad (9)
$$

where β_n are the Fourier coefficients of the function $\beta^2(\varphi)$ defined for $0 \leq \varphi \leq 2\pi$, $J_n(ka)$ is the Bessel function, and $H_n^{(1)}(ka)$ is the Hankel function of first kind.

Then by using the asymptotic behavior of cylindrical functions, the above DSE can be reduced to canonical form as follows:

$$
\sum_{n=-\infty}^{\infty} x_n |n| e^{in\varphi} = \sum_{n=-\infty}^{\infty} f_n e^{in\varphi}, \quad \varphi \in M
$$
$$
\sum_{n=-\infty}^{\infty} x_n e^{in\varphi} = 0, \quad \varphi \in S \qquad (10)
$$

where we have denoted

$$
\begin{aligned}
f_n = &- x_n \Delta_n + i\pi \sum_{p=-\infty}^{\infty} x_p \\
&\times \Big[-pn h_{n(-p)} + (ka)^2 J_p(ka) H_p^{(1)}(ka) \beta_{n-p} \\
&+ (ka)^2 g_{n(-p)} \Big] - 2z_n.
\end{aligned}
\tag{11}
$$

If coefficients f_n were known, this canonical DSE is solved analytically [9]–[12], therefore in our case the result is the following infinite matrix equation of the second kind:

$$
(I+A)X = B, \quad A = A^1 + A^2 + A^3 + A^4
\tag{12}
$$

where

$$
\begin{aligned}
&\bar{I}_{mn} = \delta_{mn}, \quad A_{mn}^1 = \Delta_n \widetilde{T}_{mn} \\
&A_{mn}^2 = i\pi n \sum_{p=-\infty}^{\infty} \widetilde{T}_{mp} p h_{p(-n)} \\
&A_{mn}^3 = -i\pi(ka)^2 J_n(ka) H_n^{(1)}(ka) \sum_{p=-\infty}^{\infty} \widetilde{T}_{mp} \beta_{p-n} \\
&A_{mn}^4 = -i\pi(ka)^2 \sum_{p=-\infty}^{\infty} \widetilde{T}_{mp} g_{p(-n)} \\
&B_m = -2 \sum_{p=-\infty}^{\infty} z_p \widetilde{T}_{mp} \\
&\Delta_n = i\pi |n|^2 J_n(ka) H_n^{(1)}(ka) - |n| \\
&m, n = 0, \pm1, \pm2, \ldots.
\end{aligned}
\tag{13}
$$

Here, $\tilde{T}_{mn} = (-1)^{m+n} T_{mn}(\cos\theta_e)$, and the T_{mn} functions can be found in [11], [13] as combinations of the Legendre polynomials (coinciding with $m^{-1} V_{m-1}^{n-1}$ of [9]). One can verify that the matrix operators $\overline{A}_{mn}^i$, $i = 1, 2, 3, 4$ have bounded norms in l_2 provided that C is a twice-differentiable curve, i.e., then $\sum_{n=-\infty}^{\infty} \sum_{m=-\infty}^{\infty} |A_{mn}^i|^2 < \infty$, $i = 1, 2, 3, 4$. Furthermore, provided that the source branch-cut B does not cross arc M, the right-hand-part elements also belong to l_2, i.e., $\sum_{m=-\infty}^{\infty} |B_m|^2 < \infty$. In this case the infinite matrix equation (12) is of the Fredholm second kind. Hence the Fredholm theorems guarantee the existence of the unique exact solution $\hat{x} \in l_2$ and also the convergence of approximate numerical solution when truncating (12) with progressively larger sizes N_{tr}. Note, however, that not all the matrix elements vanish if $k = 0$: A_{mn}^2 remain finite and vanish only if the curve M is a circular arc (i.e., eccentricity $e = 0$). Therefore, we cannot state that (12) is a result of the static part inversion although it is still a regularized matrix equation.

III. NUMERICAL RESULTS

The above-presented formulation has been verified by computing the antenna currents, radiation patterns, and directivity plots, for various problem parameters. For a comparison, additional computer simulation was performed by using the MoM applied to MPIE. Here, the Galerkin's approach was used based on the triangular subdomain functions. The elements of the "impedance" matrix A in the MoM formulation contained double integrals, which were evaluated numerically by using the optimized routines of Matlab 6.1. To generate all these numerical results we have used a PC Pentium III computer with 256 MB RAM and windows 2000 operating system.
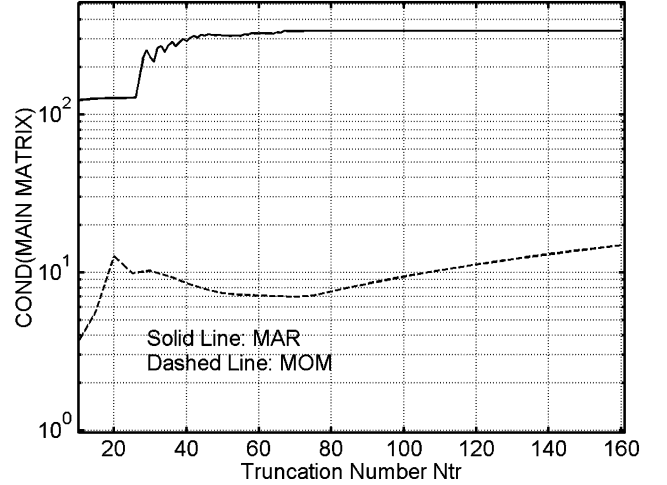

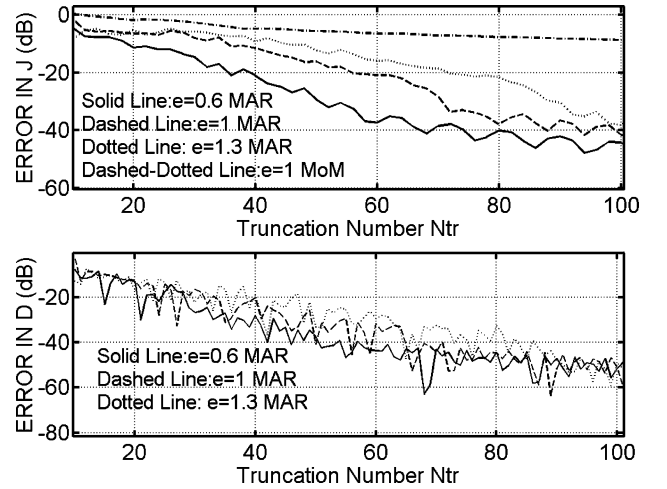Fig. 4. Condition numbers of the MoM and MAR matrices versus the truncation number N_{tr}.

Fig. 5. (a) Relative accuracy of the surface-current coefficients in terms of the truncation number N_{tr} for different eccentricity factors for the MoM and MAR cases; the other parameters are $f = 4\lambda$, $d = 10\lambda$, and $kb = 2.6$. (b) Error in directivity versus truncation number N_{tr} for different eccentricity factors; $f = 4\lambda$, the rest parameters are the same.

Fig. 4 demonstrates the condition number of the matrix versus the truncation number N_{tr}. It is seen that this value is at the reasonable level for both MAR and MoM solutions. One can also see that it has a rapidly convergent nature with the increasing of N_{tr} in the MAR case, however, in the MoM case it has a tendency to increase with larger values of N_{tr}. Besides, to verify the actual rate of convergence similarly to [12]–[18], we computed the relative error in the obtained surface current density. Here, we imply this value in the sense of so-called maximum norm, i.e., $\Delta_x = \max|x_n^{N_{tr}+1} - x_n^{N_{tr}}| / \max|x_n^{N_{tr}}|$. Fig. 5(a) presents the Δ_x plotted versus N_{tr} in logarithmic scale for different eccentricity factors e. As expected, the results display a decaying nature with greater N_{tr} values. Furthermore we can say that the greater e values entail solving of the larger-size matrix equation for the same fixed accuracy. Another parameter demonstrating the error in the far field is defined as the relative accuracy in directivity i.e., $\Delta D = |D^{N_{tr}+1} - D^{N_{tr}}| / |D^{N_{tr}}|$—see Fig. 5(b). As expected, this quantity decays faster than the near-field error. Practically speaking, four-digit accuracy in the current computation leads to the five-digit accuracy in the directivity computation. In general, these results support the convergence of our solution. When computing the g_{nm}
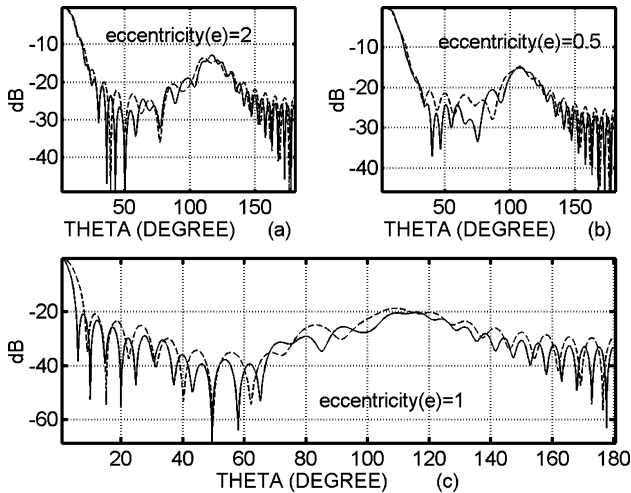
Fig. 6.   Comparison of the radiation patterns obtained with presented MAR solution for (a) hyperbolic, (b) elliptic, and (c) parabolic reflectors. Reflector parameters are $d = 12\lambda$, $f/\lambda = 6$ (solid line) and $d = 8\lambda$, $f/\lambda = 4$ (dotted line), so that $f/d = 0.5$. Feed parameter is $kb = 2$, so that the edge illumination is -7.30 dB for hyperbola, -7.90 dB for parabola and -8.78 dB for ellipse.
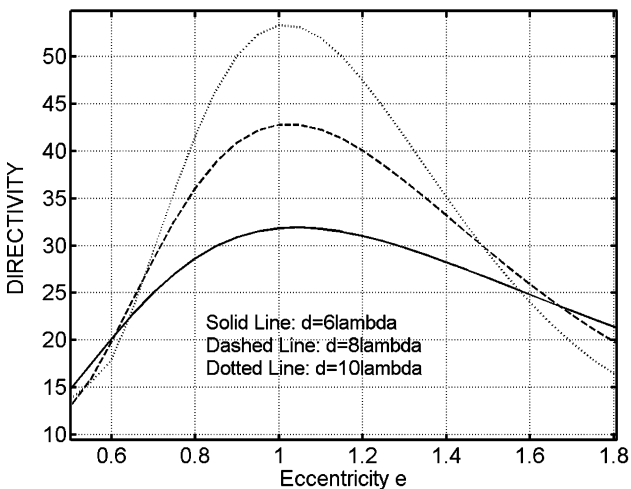

Fig. 7.   Variation of the directivity with respect to the eccentricity factor e for different aperture dimensions d/λ. The other problem parameters are $f/d = 0.5$ and $kb = 2$. Edge illumination changes from -8.79 dB ($e = 0.5$) to -7.38 dB ($e = 1.8$).

and h_{nm} coefficients, FFT algorithm was used with the order of 1024×1024. Furthermore Fig. 5 shows that the truncation number N_{tr} has to be greatly increased to obtain a reasonable accuracy in the MoM solution, however, Fig. 4 says that this entails high condition numbers. Sample normalized radiation patterns are given in Fig. 6. Here, f/d ratio and edge illumination are taken as constant values, and the data are computed for the different aperture dimensions d/λ and the eccentricity factors. In the elliptic and hyperbolic reflector cases, the smaller and greater reflector dimensions give almost the same main beam width, so no significant difference occurs in the directivity. However, in the parabolic case a larger aperture better collimates the main beam, and hence an increase in the directivity is observed.

In Fig. 7, the directivity versus eccentricity factor e is plotted for the various aperture dimensions. As expected, the directivity becomes maximum in the parabolic case ($e = 1$) and drops to small values away from the parabola. Additionally, similar curves are also plotted for the higher aperture dimensions. It is seen that the directivity increases around parabolic case with the increasing d/λ. Away from parabola this tendency of linear increase disappears and only some small variations occur. This situation is in agreement with the results in Fig. 6.

IV. CONCLUSION

A 2-D reflector antenna illuminated with a directive feed has been modeled by the CSP-RHP approach for the H-polarization case. This is a continuation of our similar study performed for the E-polarization in [18]. In computations, reflector contour was given by a conical section profile. Efficient computation of the double Fourier series coefficients of smooth functions appearing after the kernel singularity extraction is one of the important technical problems of this method, and we have solved it by using the FFT algorithm. All this enabled us to analyze electrically larger reflectors that are normally not accessible with MoM. The plots of the computational error versus the truncation number support the convergence statement. Radiation characteristics of the studied system have been examined by computing the radiation patterns and directivity for various problem parameters. Presented results justify the basic conclusions of the practical antenna engineering.

REFERENCES

[1] J. D. Kraus and R. J. Marhefka, *Antennas: For All Applications*.   New York: McGraw-Hill, 2002.
[2] G. A. Suedan and E. V. Jull, "Beam diffraction by planar and parabolic reflectors," *IEEE Trans. Antennas Propagat.*, vol. 39, pp. 521–527, Apr. 1991.
[3] L. B. Felsen, "Complex source point solutions of the field equations and their relation to the propagating and scattering of Gaussian beams," in *Symp. Math.*   New York: Academic Press, 1976, vol. 18, pp. 39–56.
[4] M. Idemen and A. Büyükaksoy, "High frequency surface currents induced on a perfectly conducting cylindrical reflector," *IEEE Trans. Antennas Propagat.*, vol. AP-32, pp. 501–507, 1984.
[5] J. R. Mautz and R. F. Harrington, "Electromagnetic penetration into a conducting circular cylinder through a narrow slot, TE case," *J. Electromagn. Waves Applicat.*, vol. 3, no. 4, pp. 307–336, 1989.
[6] D. G. Dudley, "Error minimization and convergence in numerical methods," *Electromagn.*, vol. 5, no. 2–3, pp. 89–97, 1985.
[7] A. I. Nosich, "MAR in the wave-scattering and eigenvalue problems: foundations and review of solutions," *IEEE Antennas Propagat. Mag.*, vol. 42, no. 3, pp. 34–49, 1999.
[8] W. Y. Yin, L. W. Li, T. S. Yeo, and M. S. Leong, "Multiple penetration of a $\mathbf{TE}_z$-polarized plane wave into a multilayered cylindrical cavity-backed aperture," *IEEE Trans. Electromagn. Compatibility*, vol. 42, pp. 330–337, Nov. 2000.
[9] Z. S. Agranovich, V. A. Marchenko, and V. P. Shestopalov, "Diffraction of a plane electromagnetic wave from plane metallic lattices," *Soviet Phys. Techn. Phys.*, vol. 7, pp. 277–286, 1962.
[10] V. N. Koshparenok and V. P. Shestopalov, "Diffraction of a plane electromagnetic wave by a circular cylinder with a longitudinal slot," *USSR J. Computat. Mathem. Mathem. Physics*, vol. 11, no. 3, pp. 222–243, 1971.
[11] A. I. Nosich *et al.*, "Green's function—dual series approach in wave scattering from combined resonant scatterers," in *Analytical and Numerical Methods in Electromagnetic Wave Theory*, M. Hashimoto *et al.*, Eds.   Tokyo, Japan: Science House, 1993, pp. 419–469.
[12] A. Altintas and A. I. Nosich *et al.*, "The method of regularization and its application to some electromagnetic problems," in *Applied Computational Electromagnetics*. ser. NATO-ASI Series F, N. Uzunoglu *et al.*, Eds.   Berlin, Germany: Springer, 1999, pp. 409–423.
[13] T. Oğuzer, A. Altintas, and A. I. Nosich, "Accurate simulation of reflector antennas by the complex source—dual series approach," *IEEE Trans. Antennas Propagat.*, vol. 43, pp. 793–802, Aug. 1995.
[14] A. I. Nosich and V. B. Yurchenko, "Numerically exact analysis of a two-dimensional variable-resistivity reflector fed by a complex point source," *IEEE Trans. Antennas Propagat.*, vol. 45, pp. 1592–1601, Nov. 1997.
[15] V. B. Yurchenko, A. Altintas, and A. I. Nosich, "Numerical optimization of a cylindrical reflector-in-radome antenna system," *IEEE Trans. Antennas Propagat.*, vol. 47, pp. 668–673, Apr. 1999.
[16] T. Oğuzer, "Analysis of circular reflector antenna covered by concentric dielectric radome," *IEEE Trans. Antennas Propagat.*, vol. 49, pp. 458–463, Mar. 2001.

[17] S. V. Boriskina, A. I. Nosich, and A. Altintas, "Effect of the imperfect flat earth on the vertically polarized radiation of a cylindrical reflector antenna," *IEEE Trans. Antennas Propagat.*, vol. 48, pp. 285–293, Feb. 2000.

[18] T. Oğuzer, A. I. Nosich, and A. Altintas, "E-polarized beam scattering by an open cylindrical PEC strip having arbitrary conical-section profile," *Microwave Optical Technology Letters*, vol. 31, no. 6, pp. 480–484, 2001.

[19] A. I. Nosich and S. V. Boriskina, "MAR in the problems of wave diffraction by dielectric cylinders of arbitrary cross-sections," *Radio Physics and Radio Astronomy*, vol. 3, no. 4, pp. 405–413, 1998.

[20] Y. A. Tuchkin, "Wave scattering by an open cylindrical screen of arbitrary profile with the Dirichlet boundary condition," *Soviet Physics Doklady*, vol. 30, pp. 1027–1030, 1985.

[21] ——, "Wave scattering by an open cylindrical screen of arbitrary profile with the Neumann boundary condition," *Soviet Physics Doklady*, vol. 32, pp. 213–214, 1987.

[22] V. Veremey and A. Poyedinchuk, "Two-dimensional scattering from a cavity-backed aperture with resonant loading," in *Proc. IEEE APS-URSI Int. Symp. Digest*, Chicago, IL, 1994, pp. 1090–1093.

[23] J. Mosig and F. Gardiol, "General integral-equation formulation for microstrip antennas and scatterers," *Proc. Inst. Elect. Eng.*, pt. H, vol. 132, pp. 424–432, 1985.

[24] J. Saranen and G. Vainikko, "Trigomometric collocation method with product integration for boundary integral equations on closed curves," *SIAM J. Numer. Anal.*, vol. 33, no. 4, pp. 1577–1596, 1996.

[25] N. Morita, N. Kumagai, and J. R. Mautz, *Integral Equation Methods for Electromagnetics*. Boston, MA: Artech House, 1990.